Journal of Power Sources 242 (2013) 255–263

Contents lists available at SciVerse ScienceDirect

Journal of Power Sources

journal homepage: www.elsevier.com/locate/jpowsour

Fabrication of highly porous platinum electrodes for micro-scale applications by pulsed electrodeposition and dealloying

Christian Köhler [a], Arne Kloke [a], Anna Drzyzga [a], Roland Zengerle [a,b], Sven Kerzenmacher [a,*]

[a] IMTEK – Department of Microsystems Engineering, University of Freiburg, Georges-Koehler-Allee 103, 79110 Freiburg, Germany
[b] BIOSS – Centre for Biological Signalling Studies, University of Freiburg, 79110 Freiburg, Germany

HIGHLIGHTS

- Mechanically stable platinum electrodes with roughness factors of up to RF = 6500.
- Electrodeposition method advantageous for applications such as micro fuel cells.
- Higher current for the oxidation of formic acid and glucose than state-of-the-art.
- Methanol oxidation current comparable to commercial electrodes.

ARTICLE INFO

Article history:
Received 21 February 2013
Received in revised form
2 May 2013
Accepted 11 May 2013
Available online 18 May 2013

Keywords:
Implantable glucose fuel cell
Fuel cell
Platinum electrodes
Methanol
Formic acid
Electrodeposition

ABSTRACT

We present the implementation and optimization of a novel electrodeposition method for the fabrication of highly porous platinum electrodes. It is based on the co-deposition of platinum and copper and the selective dealloying of copper in a pulsed manner. The new process yields mechanically stable platinum electrodes with roughness factors of up to RF = 6500 ± 700, compared to the state-of-the-art cyclic electrodeposition method this corresponds to an improvement in RF by 111%. Furthermore the time demand for fabrication is reduced by 59%, whereas the platinum utilization is increased by 53%. The method is particularly advantageous for applications such as micro fuel cells since it enables the precise deposition of catalytically active electrodes on micro-structured conductive areas. In this context the novel platinum electrodes show higher current densities for the oxidation of formic acid and glucose than state-of-the-art electrodes. In terms of methanol oxidation their catalytic activity is comparable to commercial direct methanol fuel cell (DMFC) electrodes, fabricated from Pt–Ru nanoparticles dispersed on carbon black.

1. Introduction

1.1. Applications of porous platinum electrodes

Since porous platinum electrodes combine high catalytic activity and high specific surface area in one material their fabrication is of great interest for a broad range of applications [1,2]. For instance in small and micro-scale fuel cells porous platinum electrodes find use as catalysts for the electro-oxidation of methanol [3–5], ethanol [6], formic acid [7,8] or glucose [9–13] as well as the electro-reduction of oxygen [12–14]. A further field of application for porous platinum is electrochemical detection, where it is used as sensor electrode for glucose [15–18], dissolved oxygen [19], pH [20], hydrogen peroxide [21], hydrogen [22] or other gasses [23,24]. Its high biocompatibility and chemical stability renders porous platinum often first choice as catalyst material for body-implantable applications [1]. One example is electrodes for implantable glucose fuel cells [9,10,12,25,26], where a high specific catalyst surface promotes the kinetically limited glucose oxidation reaction. In neural stimulation electrodes [27–29], the electrode-electrolyte impedance is inversely proportional to the electrode surface area, which results in higher signal quality for higher specific surface area [29].

1.2. Fabrication of porous platinum electrodes on the micro-scale

For hydrogen or direct methanol fuel cells the immobilization of platinum nanoparticles on high-surface area support materials

* Corresponding author. Tel.: +49 761 203 73218; fax: +49 761 203 73299.
E-mail addresses: christian.koehler@imtek.de (C. Köhler), arne.kloke@hsg-imit.de (A. Kloke), anna-drzyzga@web.de (A. Drzyzga), roland.zengerle@imtek.de (R. Zengerle), sven.kerzenmacher@imtek.de (S. Kerzenmacher).

0378-7753/$ – see front matter © 2013 Elsevier B.V. All rights reserved.
http://dx.doi.org/10.1016/j.jpowsour.2013.05.035

such as carbon black is an established method [1,30,31]. Such approaches, in which individual particles are formed to an ink together with e.g. polymer binders have the advantage of high platinum utilization [32] and are well suited for large-scale applications. However, in micro-scale applications such as micro fuel cells for the oxidation of methanol, ethanol or formic acid [33–36] and stimulation or sensor electrodes [27–29] an ink-based electrode fabrication may be difficult to implement. In this context electrodeposition would be advantageous since it enables the precise deposition of catalytically active electrodes on micro structured conductive areas [33,36].

Recently Kloke et al. [12,13] introduced a cyclic electrodeposition procedure based on cyclic voltammetry (CV) to fabricate porous platinum electrodes with roughness factors (RF, ratio between active surface area and geometrical base area) of up to 3100. During CV scans in an acidic electrolyte containing platinum and copper the co-deposition of PtCu and the selective dissolution of the less noble Cu are repeated, leading to the formation of mechanically stable porous platinum electrode. The main drawback of their approach is that although the fabrication process only requires two small potential windows for deposition and dissolution, the potential is swept over a much larger range during the CV cycle. Consequently, the time demand of this method is much higher than necessary. Furthermore, they used silicon substrate onto which a conductive seed layer of platinum was evaporated. Due to the semiconducting nature of the silicon substrate, this required additional masking to prevent the undesired formation of non-adherent platinum particles on parts of the underlying silicon substrate exposed to the electrolyte.

In the present work we show the transferability of the cyclic electrodeposition method to time-efficient pulsed electrodeposition on a ceramic substrate that requires no cumbersome masking. The design of experiments (DOE) method is used to identify the relevant process parameters and to further increase the specific surface area of the platinum electrodes. Their performance for the electro-oxidation of methanol, formic acid, and glucose is characterized by means of cyclic voltammetry and chronoamperometry, and compared to state-of-the-art electrodes.

2. Design of experiments

2.1. Process optimization by design of experiments

Design of experiments (DOE) is a statistical method to reduce the number of experiments required for the analysis of a process or to predict the behavior of complex systems [37–42]. It can be used to analyze the significance of process parameters (degree of influence on the desired output) in a screening, and also to identify the correlation between process parameters and the corresponding response variables of a complex system as a response surface [39,42]. This correlation between the process parameters (also called factors or input factors) x_i ($i = 1, 2,\ldots, k$) and the response surface ς_i is approximated by a polynom with first and second order terms [38,42]:

$$\eta_i = a_0 + \sum_{i=1}^{k} a_i x_i + \sum_{i=1}^{k} a_{ii} x_i^2 + \sum_{\substack{i=1 \\ i<j}}^{k} \sum_{i=1}^{k} a_{ij} x_i x_j \qquad (1)$$

where a_i ($i = 1,2,\ldots k$) are coefficients and the summands describe linear, quadratic, and two-factor interactions of the process parameters.

To cover the parameter space of interest, an experimental design matrix has to be established, that considers a minimum and maximum value for each process parameter. For a system with three process parameters ($k = 3$) this results in a cube as illustrated exemplarily in Fig. 1A [37,38]. Here the 2^k corner points of the experimental design describe the *factorial portion*. To achieve a compromise between number of experiments and significance we chose the central composite design (CCD), in which besides the corner points also the $2k$ star points (*axial portion*) and a center point are used to cover the parameter space [37,38,40].

Since the statistical error of the response surface within the parameter space is calculated from the statistical error of the center point, its determination is essential [38,39]. To simplify the calculation of the statistical error the experimental design has to be rotatable, which means that the distance between center and star points has to be the same as the distance between center and corner points. In a rotatable design the statistical error of the response surface corresponds to the statistical error of the center point and is symmetrical. To ensure rotatability of a design the value α, which is given by the distance between star points and center point (see Fig. 1A) has to obey $\alpha = (F)^{1/4}$ (with F the number of corner or factorial points) [38]. For a complex system with 4 factors rotatability is given for $\alpha = 2$.

After establishing the experimental design matrix, the actual experiments corresponding to the individual parameter combinations of cube corner, star and center points have to be performed and their response values evaluated. To be able to quantify the statistical error, the center point was repeated 6 times and the whole experimental design matrix (30 experiments, see Supplementary Table S1) was repeated once. Out of these experimental results a regression function on basis of Equation (1) is calculated for each interaction between a parameter and the

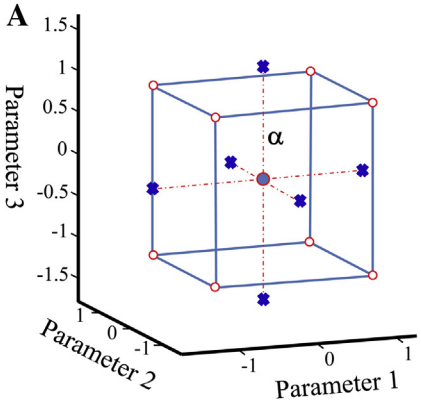

B

Process factor	Lower limit	Upper limit
Deposition potential (V vs. SCE)	-1.8	-0.2
Deposition time (s)	0.5	15
Ratio R	0.5	10
Number of pulses	50	1500

Fig. 1. A: Illustration of the central composite design (CCD) with three process factors; B: Relevant process factors and their boundary conditions as used in this work.

response. The coefficients a_i (see Eq. (1)) of these regression functions are called *parameter estimates* [43]. Together with their calculated standard errors these are used to describe the so called *t-ratio* given as:

$$t - ratio = \frac{\text{parameter estimate}}{\text{standard of error parameter estimate}} \quad (2)$$

The higher the absolute value of the *t-ratio*, the larger is the influence of the parameter on the corresponding response surface. In the present investigation a significance level of 0.05 is used, which means that only process parameters with an absolute *t-ratio* value higher than 2 are considered to have a significant influence on the response surface [43].

Commonly, the investigated problems are multi-response problems, in which it is necessary to find a trade-off between different responses. This is realized through the so called "desirability scale" [44]. For each response variable, the lower case "*d*" describes the desirability of an individual response variable. Typically the scale for *d* is between 0.00 and 1.00, in which $d = 0.00$ stands for a completely undesirable and $d = 1.00$ for a completely desirable value [44]. For a multi-response problem with *n* responses the overall desirability "*D*" (called upper case) has to be calculated from the individual desirabilities (d_n) according to Equation (3) [44,45]:

$$D = \sqrt[n]{d_1 d_2 \ldots d_n} \quad (3)$$

To maximize the responses of the complex system it is aspired to reach desirability near 1.00, resulting in the prediction of a calculated optimal value for each process parameter.

2.2. Determination of process parameters and their boundary conditions

The principle of the novel pulsed deposition process is shown schematically in Fig. 2. For the investigation of this process using DOE it is required to identify the relevant process parameters (parameters essential for process application) and their boundary conditions. Four important process parameters for the pulsed deposition of PtCu were identified: (1) the deposition potential, (2) the deposition time, (3) the ratio between deposition and dissolution time, and (4) the number of deposition pulses and (see Fig. 2). The derivation of boundary conditions for each of these process parameters is rationalized in the following and summarized in Fig. 1B.

The reasonable limits of the *deposition potential* are determined by two electrochemical processes: the upper limit has to be less negative than the redox potential of the most ignoble metal (in this case copper), whereas the lower limit is given by the strong evolution of hydrogen gas at high overpotentials [46,47]. For initial proof-of-principle experiments we chose −1.0 V vs. SCE as the deposition potential, since under this condition the deposited amount of the metals (platinum and copper) only depends on their concentration and not on the applied potential (mass-transport limited region [48]). Using this deposition potential the fabrication of a stable catalyst layer by the pulsed deposition (PD) process was successful. Consequently, we chose −1.0 V vs. SCE as the center of the potential windows for the DOE optimization. To avoid massive hydrogen evolution the lower limit of the potential range was set to −1.8 V vs. SCE. Due to symmetry reasons the upper potential limit was chosen as −0.2 V vs. SCE, which is well within the potential range in which the deposition of platinum and copper takes place (<0.25 V vs. SCE [12]).

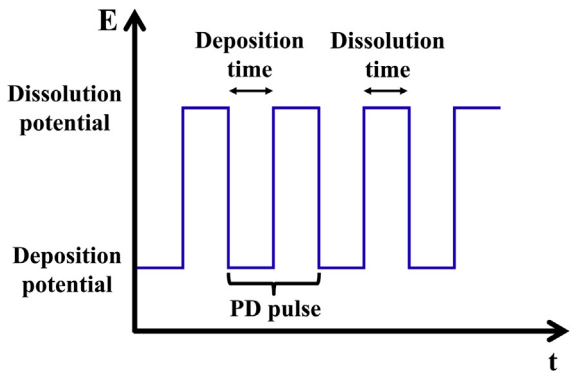

Fig. 2. Principle of the pulsed electrodeposition (PD) process and its relevant process parameters.

The *dissolution potential* was kept constant at a potential of 0.7 V vs. SCE during this investigation. This potential is in a range in which metal dissolution takes place (>0.5 V vs. SCE [12,13]), but is still below the potential of oxygen evolution at above 1.35 V vs. SCE [46].

Also the *deposition time* and the associated *ratio R* of deposition time to dissolution time defined as,

$$R = \frac{\text{dissolution time}}{\text{deposition time}} \quad (4)$$

are parameters with considerable influence on structure and stability of electrodeposited layers [47–49]. Long deposition times together with short dissolution times (low ratios) lead to a depletion of the reactant in front of the electrode, which results in dendritic structure growth but also less deposited material [1,47,48]. On the other hand the combination of short deposition time and long dissolution time (high ratios) lead to the growth of less dendritic structures due to the relaxation of the metal ion concentration inside the pores [1,47]. To cover the interplay between both parameters the deposition time was varied between 0.5 s and 15 s, whereas the ratio was varied between $R = 10$ and $R = 0.5$.

The boundary conditions for the fourth process parameter – *the number of deposition pulses* – were chosen to obtain deposition times comparable to the deposition times in the state-of-the-art cyclic electrodeposition process [12,13]. In their work Kloke et al. showed saturation of the increasing specific electrode surface area by increasing number of CV-cycles at 500 cycles [12,13], corresponding to an overall deposition time of about 4.5 h (time in which the potential is in the deposition window between 0.25 V vs. SCE and −0.6 V vs. SCE). To investigate whether such a saturation effect exists also for the PD process the lower limit of the number of pulses was chosen to 50 pulses (overall deposition time of 25 s) and the upper limit was chosen to 1500 pulses (overall deposition time of 6.25 h).

2.3. Definition and evaluation of response variables

During DOE the four process parameters (deposition potential; deposition time; number of pulses and ratio) were varied and evaluated concerning the response variables, namely the specific surface area expressed as roughness factor (RF, ratio between the electrochemically active and the geometric electrode surface, see Experimental section) and the mechanical stability of the catalyst layer.

In this investigation, the most important criterion is the maximization of the RF. Therefore was assigned the desirability of 1 to the highest RF determined in this series of experiments, and all RFs lower than 3000 were assigned to 0 (see Table 1). This lower limit

Table 1
Response variables and assigned desirability values.

Response variable	Desirability criteria	Desirability value
Roughness factor (RF)	Highest determined RF	→1
	RF < 3000	→0
Stability	Stability category: 1, 0	→1
	Stability category: −1	→0

corresponds to the RF of the state-of-the-art platinum electrodes fabricated using cyclic electrodeposition [12,13].

The required condition for the maximization of the RF is the stability of the deposited catalyst layer. The stability was categorized by a qualitative scale, which is described in detail in the Experimental section. This classification was then transferred to desirability, in which 0 stands for a completely unacceptable result and 1 for acceptable or excellent results (see Table 1).

The development of the experimental design matrix and the subsequent analysis and optimization of the experimental data was done using the software *JMP® 8.0.1* (SAS Institute Inc., Cary, USA).

3. Experimental

3.1. Deposition configuration and electrode characterization

The deposition experiments were performed using the same electrochemical configuration as described by Kloke et al., consisting of a three electrode setup, with a standard calomel electrode (SCE, KE 11, Sensortechnik Meinsberg, Ziegra-Knobelsdorf, Germany) as reference, a platinum wire (0.3 mm diameter, Chempur, Karlsruhe, Germany) as counter, and the working electrode (see Supplementary Figure S2). The electrode substrate was a ceramic wafer (4″ diameter, rubalit 710, 525 μm thickness) onto which titanium (50 nm) and platinum (250 nm) were evaporated. By a photolithography step the metallization was structured to obtain a defined deposition area of 1 cm^2 with two connection pads for separate potential and current paths (see Supplementary S3) [12,13]. To contact the working electrode platinum wires (0.1 mm diameter, Chempur, Karlsruhe, Germany) were used, which were fixed on the substrate by a sample holder consisting of polycarbonate and silicon layers as described elsewhere [50]. For the electrochemical deposition polycarbonate-frames with a 2.25 cm^2 opening were used. This prevents the accumulation of hydrogen bubbles during electrode fabrication on the central 1 cm^2 deposition area. After the deposition step the 2.25 cm^2 frame is exchanged against a 1 cm^2 frame to clearly define a 1 cm^2 electrode area.

Prior to deposition the electrodes were cleaned in sulfuric acid (0.5 M, Merck, Darmstadt, Germany) by CV (10 cycles, 50 mV s^{-1}, 1.400 to −0.400 V vs. SCE) [12,13]. The potential-controlled, pulsed electrodeposition of the platinum electrodes (a list of all parameter variation is available in the Supplementary Fig. S1) was performed under N_2 atmosphere in an electrolyte containing H_2SO_4 (0.5 M), H_2PtCl_6 (0.2 mol l^{-1}, Chempur, Karlsruhe, Germany) and $CuSO_4$ (0.02 mol l^{-1}, Merck, Darmstadt, Germany). The electrolyte volume in the deposition cell was 50 ml and the electrode was placed into a 100 ml glass beaker (see Supplementary Figure S2). A potentiostat (1470E, Solartron Analytical, Farnborough, England) was used to control the potential at the working electrode.

After the deposition step, the electrodes were cleaned during 6 cycles of CV (50 mV s^{-1}, 1.400 to −0.400 V vs. SCE) in H_2SO_4 (0.5 M). Subsequently the electrochemically active platinum surface was determined using CV in H_2SO_4 with individually adapted scan rate and negative scan limit as described elsewhere [13,51]. By this method the active surface area is determined by the desorption charge of a hydrogen monolayer and expressed as roughness factor (RF) according to

$$\mathrm{RF} = \frac{Q_{\mathrm{HDes}}}{Q_0 \times A} \tag{5}$$

where Q_{HDes} is the measured charge of the hydrogen desorption, Q_0 is the charge of a hydrogen monolayer adsorbed on polycrystalline platinum (210 μC cm^{-2}) and A is the geometric area of the electrode [51].

The electrodes were examined using scanning electron microscopy (SEM, Zeiss DSM 962) and energy-dispersive X-ray (EDX, Oxford Instruments Inca 300) to characterize the surface structure and quantify the composition of the catalyst layer, with regard to platinum and residual copper content.

3.2. Determination of catalyst stability

The stability of the electrodeposited platinum layers was qualitatively assessed by letting the electrode fall three times onto a table from a height of 5 cm for three times (see Supplementary Figure S4). By visual inspection the electrodes were assigned to the categories of −1, 0 and 1. Category "1" means that no particles dropped down from the catalyst layer (excellent stability), category "0" relates to the flaking of only a few particles (acceptable stability), and category "−1" was assigned to electrodes from which large particles peeled off (unacceptable stability). Based on this classification a desirability value between 0 and 1 (as described above) was assigned to this response variable.

3.3. Electrochemical characterization

To characterize the catalytic activity of the highly porous platinum electrodes (referred to PD–Pt) a series of cyclic voltammetry (CV) and chronoamperometry (CA) experiments were performed in acidic solutions (H_2SO_4, 0.5 M, Merck, Darmstadt, Germany) containing methanol (0.5 M, 99.5%, Carl Roth, Karlsruhe, Germany), or formic acid (0.5 M, Rotipuran 98%, Carl Roth, Germany). Experiments with glucose (3 mM, α–D (+)-glucose monohydrate 99.5%, Carl Roth, Karlsruhe Germany) were performed in a phosphate buffered saline (PBS, pH = −7.4, Invitrogen, Karlsruhe, Germany). For comparison, also commercial Pt–Ru loaded carbon electrodes for direct methanol fuel cells referred to as DMFC electrodes (Freudenberg H2315 T10A, non-woven, loading 3.0 mg cm^{-2} Pt–Ru, ratio 1:1, thickness 230 μm, Quintech, Germany), a highly porous platinum electrode fabricated by cyclic electrodeposition on silicon substrate referred to as CV–Pt [12,13], and a blank polycrystalline platinum electrode (substrate as described above without deposition) referred to as Pt_{blank} were characterized. All experiments were performed in triplicates, values are reported as mean value ± sample standard deviation.

For the CV-characterization of the *methanol oxidation* the parameters were chosen according to the investigations of Salgado and Jia et al. [3,52]. For Pt electrodes the conditions were 10 cycles, 20 mV s^{-1}, 0.855 to −0.045 V vs. SCE, and for the DMFC electrodes 0.555 to −0.045 V vs. SCE were used as potential limits, to avoid the dissolution of ruthenium at potentials higher than 0.700 mV vs. SCE [3,52,53]. The CA measurements were performed at a potential of 355 mV vs. SCE over a period of 30 min according the work of Salgado et al. [52].

For the CV-characterization of the *formic acid oxidation* the parameters were chosen according to the investigations of Lovic et al. and Rigsby et al. [7,53]. For Pt electrodes the conditions were 10 cycles, 50 mV s^{-1} 0.9 to −0.2 V vs. SCE, and for the DMFC electrodes 0.555 to −0.2 V vs. SCE were used as potential limits, to avoid the

Table 2
Influence of the process parameters (linear and quadratic) and the parameter interactions on the response variables expressed as t-ratio. Determined during DOE using the software JMP® 8.0.1.

	Term	RF (roughness factor) *t-ratio*	Stability *t-ratio*
Linear portion	Deposition potential (V vs. SCE)	−6.36	4.00
	Deposition time (s)	6.36	−6.28
	Number of pulses	7.42	0.57
	Ratio	−2.48	0.57
Quadratic portion	Deposition potential × deposition potential	−2.07	−0.46
	Deposition time × deposition time	−6.93	−0.46
	Number of pulses × number of pulses	−3.81	3.20
	Ratio × ratio	1.44	−2.29
Parameter interactions	Deposition potential × deposition time	2.91	0.70
	Deposition potential × number of pulses	1.83	0.70
	Deposition potential × ratio	−0.06	−0.70
	Deposition time × number of pulses	−2.12	2.10
	Deposition time × ratio	0.66	0.70
	Number of pulses × ratio	0.17	0.70

dissolution of ruthenium at potentials higher than 0.700 mV vs. SCE [3,52,53]. The CA measurements were performed at a potential of 400 mV vs. SCE over a period of 30 min according the work of Hwang et al. [54].

For the CV-characterization of the *glucose oxidation* parameters were chosen with respect to the work of Kloke et al. [13]. The conditions for all Pt electrodes were 10 cycles, 2 mV s^{-1}, 1.200 to −0.900 V vs. SCE. The CA measurements were performed at −0.200 V vs. SCE (corresponding to the typical potential for anodic glucose oxidation in a fuel cell [11,13]) over a period of 30 min.

4. Results & discussion

4.1. Implementation of a ceramic sample substrate

Performing the state-of-the-art cyclic electrodeposition process (500 deposition cycles, 1.400 to −0.600 V vs. SCE [12,13]) on a ceramic substrate results in electrodes with roughness factors of RF = 5000 ± 300. This is an increase by about 60% compared to the RF = 3070 ± 300 obtained under the same conditions but with a silicon substrate [12,13]. This lower RF obtained with the silicon substrate is attributed to the accumulation of hydrogen bubbles on the edges of central 1 cm^2 electrode area, caused by the polymer masking layer required to prevent platinum deposition on the semi-conducting silicon substrate [12,13]. Because of its non-conductive nature the novel ceramic substrate requires no protection layer around the central electrode area on which hydrogen bubbles formed during the deposition process could accumulate.

4.2. Dependence of the response surface on process parameters

In Table 2 the influence of the process parameters (expressed as *t-ratio*) on the response variables (RF and stability) is shown. The analysis of the *t-ratio* shows that all four process parameters have a significant influence on the RF (means the absolute values of the *t-ratio* are clearly above 2, see Table 2 middle column). For deposition time and number of pulses the *t-ratio* has a linear and a quadratic portion (see Table 2 middle column). In contrast, the deposition potential and the ratio have only a linear influence on the RF. Since the influence of most process parameter interactions on the RF is

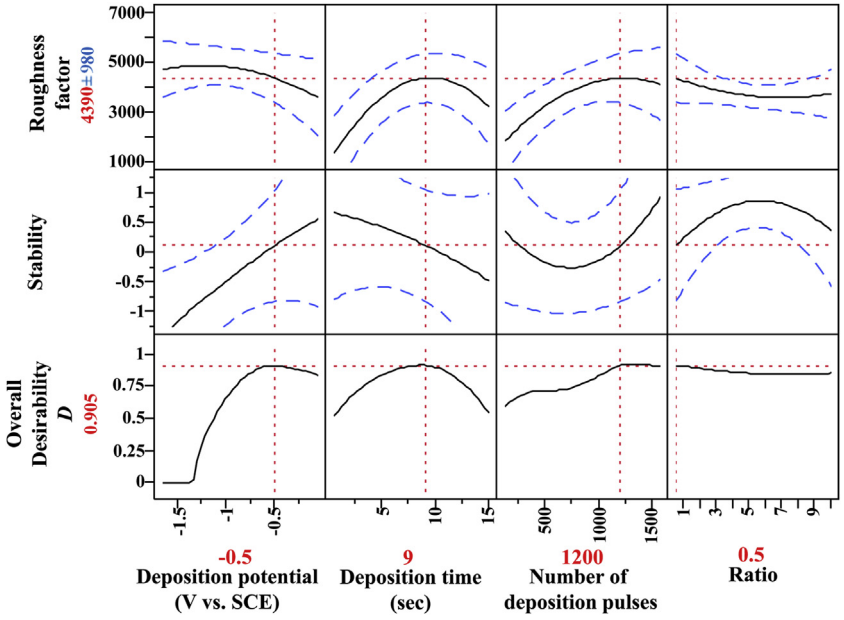

Fig. 3. Response surface of the pulsed deposition in dependence of the four process parameters (deposition potential, deposition time, number of deposition pulses and ratio). The black lines describe the predicted trend of the response according the single process parameters and the dotted blue line assign the variation. The intersection of the two red lines highlights the optimal value for the parameters and their predicted response value. (For interpretation of the references to color in this figure legend, the reader is referred to the web version of this article.)

Table 3
Optimized process parameter for the pulsed electrodeposition developed by DOE.

Process parameter	Optimal value
Deposition potential (V vs. SCE)	−0.5
Deposition time (sec)	9
Number of deposition pulses	1200
Ratio	0.5
Predicted RF from DOE	*4390 ± 980*
Experimental determined RF	*6500 ± 700*

only less pronounced (means the absolute value of the *t-ratio* is around 2, see Table 2 middle column), each parameter is variable independently from the other process parameters. This means that it is possible to keep three of the process parameters at a fixed value, while by varying the fourth parameter the influence of only this parameter on the response surface is directly detectable and thus optimizable. The interaction of *deposition potential* × *deposition time* shows the highest *t-ratio* (2.91), but also this value is negligible small compared to the linear and quadratic *t-ratios*.

Regarding the catalyst stability only the deposition time (*t-ratio* = −6.28) and the deposition potential (*t-ratio* = 4.00) show a significant influence, which is linear (see Table 2). The influence of the number of pulses on the stability shows a minimum and the ratio shows a maximum resulting from their quadratic *t-ratio* portion and no linear dependence (see Table 2 right column). Similar to the RF also for the catalyst stability no process parameter interaction shows a significant influence (means all *t-ratio* around values of 2, see Table 2).

4.3. Maximization of the roughness factor

In Fig. 3 the response surface of the PD process in dependence of the individual process parameters is shown. To maximize the response variable RF the optimal value for every single process parameter has to be identified with respect to the defined desirability *d* of each response variable (see Table 1). Hence for each process parameters the highest *d* has to be identified out of the calculated regression function (see Fig. 3). Out of these single *d*'s the overall desirability *D* can be calculated (see Equation (3)).

Regarding the development of the RF in dependence of the deposition potential a predicted maximum at a potential of about −1.25 V vs. SCE is found (see Fig. 3 left). However, the stability of the catalyst layer decreases with decreasing the deposition potential. With the use of the desirability function the maximal overall desirability (means the highest possible RF with a stable catalyst layer) of $D = 0.905$ results for a deposition potential of −0.5 V vs. SCE. For lower deposition potentials the desirability decreases massively due to the instability of the deposited catalyst layer.

In contrast, regarding the other parameters deposition time and number of deposition pulses the optimal value for a maximal RF also shows the highest overall desirability. Regarding the ratio *R* no global maximum for the RF within the chosen boundary conditions is found, the highest RF is obtained for the lowest ratio of 0.5.

In Table 3 the predicted optimal values for the single process parameters and the predicted response for the maximum RF are shown. The experimental verification (24 repetitions) of the predicted optimized process parameters yielded stable electrodes with a roughness factor of RF = 6500 ± 700. Considering the relatively small number of DOE experiments this value is in reasonable agreement with the predicted maximum RF (4390 ± 980).

Because the response surface analysis (see Fig. 3 right) shows no global maximum in the predicted RF within the chosen limits of the ratio it is necessary to perform an additional investigation to identify the global maxima of that process factor. During the experiment the other three factors are kept at their determined, optimal values (see Table 3) and the boundary conditions for the ratio were expanded from the DOE range (0.5–10) to 0.1 to 15. All investigated parameter for the ratio were repeated twice. For values lower than 0.5 and higher than 10, the RF decreased or showed even a non-stable catalyst layer. Compared to the DOE optimization results thus no higher RF could be obtained.

In Fig. 4 electron micrographs of the PD–Pt electrodes fabricated with the optimized process parameters are shown. As can be seen, the electrodes exhibit a cauliflower-like structure, similar to the previous CV–Pt electrodes [12,13]. The maximized RF of the novel porous platinum electrodes (6500 ± 700) shows an increase of about 30% compared to the cyclic electrodeposition on a ceramic substrate, and an increase of about 111% compared to the state-of-the-art electrodes presented by Kloke et al. [12,13]. The time demand for the fabrication of the porous catalyst layer is reduced by 59%. The EDX analysis revealed a twice as high remaining copper content of about in the PD–Pt electrodes (28 at-%) compared to state-of-the-art CV–Pt electrodes (about 14 at-%). Furthermore the platinum utilization calculated according to Kloke et al. corresponds to 11.5%, which is about 53% higher than state-of-the-art CV–Pt electrodes (7.5%) [13].

4.4. Catalytic activity of PD-electrodes for oxidation of methanol, formic acid and glucose

Fig. 5A shows the CV for the methanol oxidation of the different tested electrodes. The oxidation current densities of

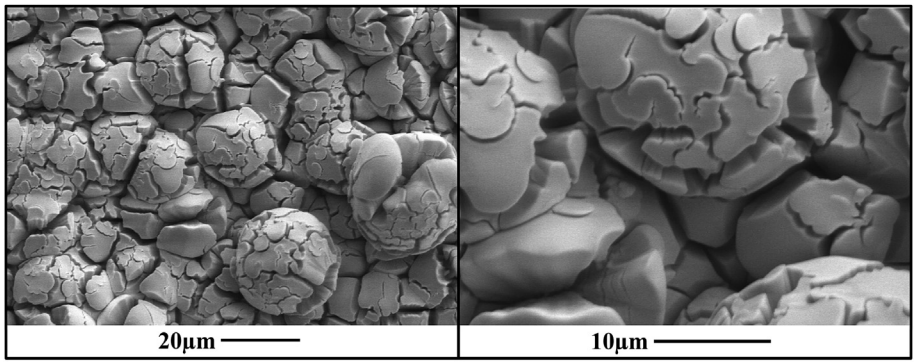

Fig. 4. SEM pictures of a porous platinum electrodes fabricated using pulsed electrodeposition (1200 pulses, −0.5/0.7 V vs. SCE, 9 s, $R = 0.5$).

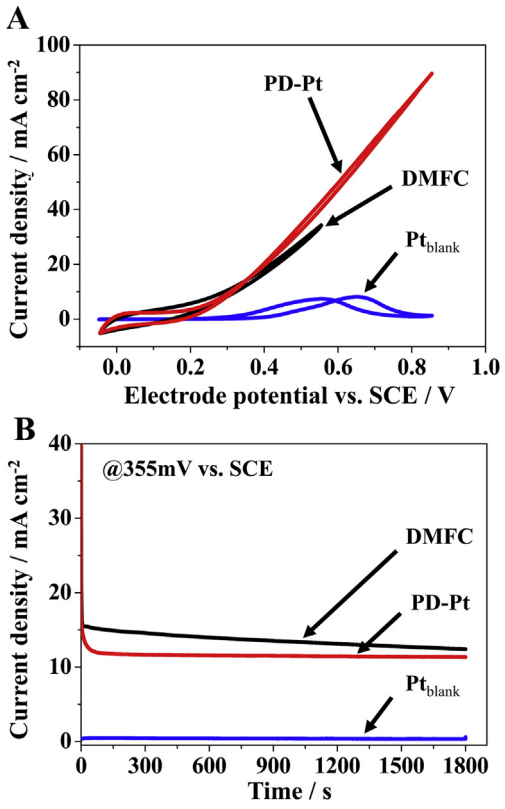

Fig. 5. Electrochemical investigation of the methanol oxidation on platinum-based catalysts. A shows the stable 10th cycle of the CV (20 mV s^{-2}) in acidic solution containing 0.5 M methanol of the three different electrodes (Pt_{blank}; DMFC and PD–Pt) and B shows the current response of a potentiostatic measurement at 355 mV vs. SCE in the same solution.

DMFC and PD–Pt electrodes are comparable, amounting to 14.8 ± 1.9 mA cm^{-2} (DMFC) and 14.3 ± 0.8 mA cm^{-2} (PD–Pt) at a potential of 0.355 V vs. SCE. This is in agreement with the CA experiment at 0.355 V vs. SCE (see Fig. 5B). After a period of 1800 s the current densities of the DMFC electrodes were 12.4 ± 0.3 mA cm^{-2}, and the PD–Pt electrodes showed 11.4 ± 0.3 mA cm^{-2} (see Fig. 5B). That means that at the end of the experiment the current density of the PD–Pt electrodes was only 8% lower compared to the DMFC electrode. Remarkably, the DMFC electrode shows a higher decrease in current density than the PD–Pt electrode during the experimental period. Future research is required to clarify whether this stems from an improved poisoning resistance of the PD–Pt catalyst or is related to an improved CO_2-transport in our electrode structure. In all cases the Pt_{blank} showed low or even negligible current densities demonstrating the catalytic activity of the here fabricated highly porous platinum electrodes.

In Fig. 6 the investigation of the oxidation of formic acid during the CV and CA experiments is shown. During CV the PD–Pt electrodes show 42.7 ± 9.8 mA cm^{-2} at a potential of 400 mV vs. SCE. This is a by 70% higher oxidation current density than that of the commercial DMFC electrode (25.3 ± 6.3 mA cm^{-2}). This result is confirmed by the CA experiments (about 53% higher oxidation current density). Within the investigation period of 30 min the DMFC electrodes show a pronounced decrease of the current density, which is not observed with the novel PD–Pt electrodes (see Fig. 6B). To clarify whether this results from lower poisoning of the PD–Pt catalyst or improved CO_2-transport in the PD–Pt electrode structure has to be investigated in further experiments beyond the

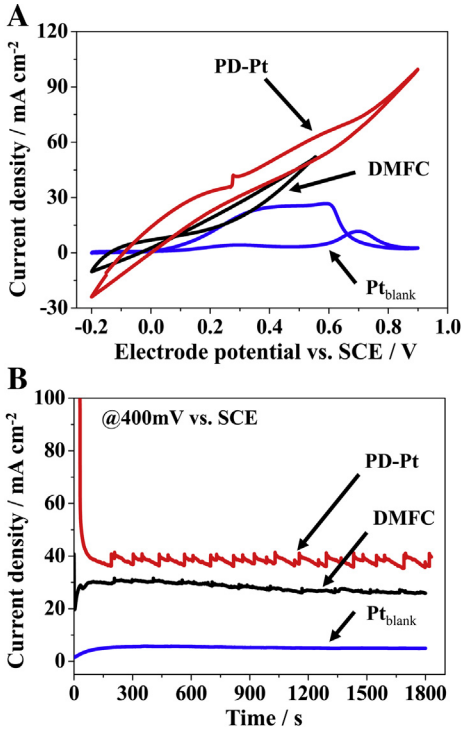

Fig. 6. Electrochemical investigation of the formic acid oxidation on platinum-based catalysts. A shows the stable 10th cycle of the CV (50 mV s^{-2}) in acidic solution containing 0.5 M formic acid of the three different materials (Pt_{blank}; DMFC and PD–Pt) and B shows the current response of a potentiostatic measurement at 400 mV vs. SCE in the same solution.

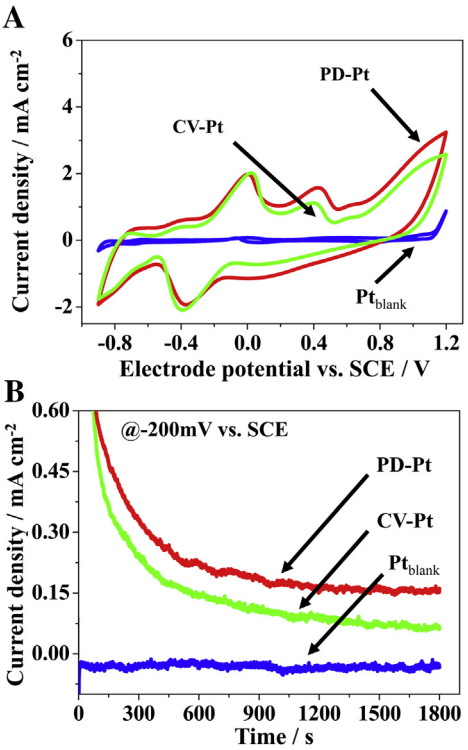

Fig. 7. Electrochemical investigation of the glucose oxidation on platinum-based catalysts. A shows the stable 10th cycle of the CV (2 mV s^{-2}) in phosphate buffered saline containing 3 mM glucose of the three different materials (Ptblank; CV–Pt and PD–Pt) and B shows the current response of a potentiostatic measurement at −200 mV vs. SCE in the same solution.

scope of the present work. During all investigations the Pt_{blank} shows only low oxidation current density, demonstrating the catalytic activity of the here fabricated highly porous platinum electrodes.

Fig. 7 compares the CV and CA results of the oxidation of glucose CV–Pt & PD–Pt electrodes. In the CV-experiments both porous platinum electrodes show comparable current densities and at a potential of −200 mV vs. SCE, amounting to 78 ± 6 μA cm^{-2} (CV–Pt) and 85 ± 12 μA cm^{-2} (PD–Pt). At the beginning of the CA experiment (see Fig. 7B) the CV–Pt electrodes show comparable currents to the PD–Pt electrodes, but in case of CV–Pt the current decrease over time is much more pronounced. After 1800 s of constant potentiostatic load the state-of-the-art CV–Pt electrodes exhibit only oxidation currents of 62 ± 25 μA cm^{-2}, whereas the PD–Pt electrodes showed still 155 ± 53 μA cm^{-2}. The Pt_{blank} electrodes showed only reductive currents (meaning negative currents) during the CA experiment. This reductive currents result from residual oxygen in the media, because these low specific surface area platinum electrodes show a high oxygen-sensitivity [13].

5. Conclusion

In this work we demonstrate the fabrication of highly porous platinum electrodes by a novel process based on the co-deposition of platinum and copper and the selective dealloying of copper in a pulsed manner. The new process is particularly advantageous for micro-scale applications such as micro fuel cells for the oxidation of methanol or formic acid [33–36] and stimulation or sensor electrodes [27–29] since it enables the precise deposition of catalytically active electrodes on micro structured conductive areas [33,36].

Compared to the state-of-the-art electrodes fabricated by cyclic electrodeposition [12,13] our new approach has the advantages of a by 111% increased specific electrode surface area (RF = 6500 ± 700), and a by 59% reduced time demand. Furthermore the platinum utilization of 11.5% is by about 53% higher compared to state-of-the-art cyclic electrodeposition electrodes (7.5%) [13]. The novel electrodes exhibit high catalytic activity and are of applicational relevance for micro-scale fuel cells using methanol, formic acid, or glucose as the fuel. Compared to state-of-the-art electrodes their steady state current densities for the oxidation of formic acid and glucose are by 53% and 250% higher. In the case of methanol oxidation, they exhibit current densities that are comparable to commercial DMFC electrodes fabricated from Pt–Ru nanoparticles dispersed on carbon black, but their current density development over time is more stable. Whether this results from higher poisoning resistance or improved CO_2-transport in the novel PD–Pt electrode structure, has to be clarified in further experiments beyond the scope of the present work. In this context, it has to be considered that that the novel platinum catalyst has still a remaining copper content of about 28 at-%. As described by Strasser and co-workers [55–57], embedded copper can effect a change in electrocatalytic activity due to a reduced interatomic Pt–Pt distance and changes in the electronic structure in the platinum-rich surface region.

Acknowledgment

This study was supported by the German Research Association DFG (GRK 1322).

Appendix A. Supplementary data

Supplementary data related to this article can be found at http://dx.doi.org/10.1016/j.jpowsour.2013.05.035.

References

[1] A. Kloke, F. von Stetten, R. Zengerle, S. Kerzenmacher, Adv. Mater. 23 (2011) 4976–5008.
[2] A.C. Chen, P. Holt-Hindle, Chem. Rev. 110 (2010) 3767–3804.
[3] J.B. Jia, L.Y. Cao, Z.H. Wang, Langmuir 24 (2008) 5932–5936.
[4] C. Coutanceau, A.F. Rakotondrainibe, A. Lima, E. Garnier, S. Pronier, J.M. Leger, C. Lamy, J. Appl. Electrochem. 34 (2004) 61–66.
[5] E. Antolini, T. Lopes, E.R. Gonzalez, J. Alloys Compd. 461 (2008) 253–262.
[6] X.Y. Zhang, W. Lu, J.Y. Da, H.T. Wang, D.Y. Zhao, P.A. Webley, Chem. Commun. (2009) 195–197.
[7] J.D. Loviç, A.V. Tripkoviç, S.Lj. Gojkoviç, K.D. Popoviç, D.V. Tripkoviç, P. Olszewski, A. Kowal, J. Electroanal. Chem. 581 (2005) 294–302.
[8] N. Kristian, Y.L. Yu, P. Gunawan, R. Xu, W.Q. Deng, X.W. Liu, X. Wang, Electrochim. Acta 54 (2009) 4916–4924.
[9] S. Kerzenmacher, J. Ducrée, R. Zengerle, F. von Stetten, J. Power Sources 182 (2008) 1–17.
[10] S. Kerzenmacher, U. Kräling, T. Metz, J. Ducrée, R. Zengerle, F. von Stetten, J. Power Sources 196 (2011) 1264–1272.
[11] S. Kerzenmacher, M. Schroeder, R. Brämer, R. Zengerle, F. von Stetten, J. Power Sources 195 (2010) 6516–6523.
[12] A. Kloke, C. Köhler, R. Zengerle, S. Kerzenmacher, Adv. Mater. 24 (2012) 2916–2921.
[13] A. Kloke, C. Koehler, R. Zengerle, S. Kerzenmacher, J. Phys. Chem. C (2012).
[14] S. Kerzenmacher, U. Kräling, M. Schroeder, R. Brämer, R. Zengerle, F. von Stetten, J. Power Sources 195 (2010) 6524–6531.
[15] J.H. Yuan, K. Wang, X.H. Xia, Adv. Funct. Mater. 15 (2005) 803–809.
[16] D. Rathod, C. Dickinson, D. Egan, E. Dempsey, Sens. Actuators B Chem. 143 (2010) 547–554.
[17] J.J. Li, R. Yuan, Y.Q. Chai, X. Che, W.J. Li, X. Zhong, Microchim. Acta 172 (2011) 163–169.
[18] Q. Xu, L. Yin, C. Hou, X. Liu, X. Hu, Sensors Actuators B Chem. 173 (2012) 716–723.
[19] Y.J. Lee, J.Y. Park, J. Korean Phys. Soc. 58 (2011) 1505–1510.
[20] J. Noh, S. Park, H. Boo, H.C. Kim, T.D. Chung, Lab. Chip 11 (2011) 664–671.
[21] Y.J. Lee, J.Y. Park, Y. Kim, J.W. Ko, Curr. Appl. Phys. 11 (2011) 211–216.
[22] G. Korotcenkov, S. Do Han, J.R. Stetter, Chem. Rev. 109 (2009) 1402–1433.
[23] B. Pejcic, P. Eadington, A. Ross, Environ. Sci. Technol. 41 (2007) 6333–6342.
[24] P. Jacquinot, B. Muller, B. Wehrli, P.C. Hauser, Anal. Chim. Acta 432 (2001) 1–10.
[25] V. Oncescu, D. Erickson, J. Power Sources 196 (2011) 9169–9175.
[26] B.I. Rapoport, J.T. Kedzierski, R. Sarpeshkar, PLoS One 7 (2012) e38436.
[27] T. Boretius, T. Jurzinsky, C. Köhler, S. Kerzenmacher, H. Hillebrecht, T. Stieglitz, in: Proceedings of the 33rd Annual International Conference of the IEEE Engineering in Medicine and Biology Society (EMBC '11), Boston (2011) 5404–5407.
[28] E.M. Hudak, J.T. Mortimer, H.B. Martin, J. Neural Eng. 7 (2010).
[29] S. Mailley, M. Hyland, P. Mailley, J.A. McLaughlin, E.T. McAdams, Bioelectrochemistry 63 (2004) 359–364.
[30] Z.M. Peng, H. Yang, Nano Today 4 (2009) 143–164.
[31] A.R. Tao, S. Habas, P.D. Yang, Small 4 (2008) 310–325.
[32] E.A. Ticianelli, C.R. Derouin, A. Redondo, S. Srinivasan, J. Electrochem. Soc. 135 (1988) 2209–2214.
[33] E. Kjeang, N. Djilali, D. Sinton, J. Power Sources 186 (2009) 353–369.
[34] S. Sundarrajan, S.I. Allakhverdiev, S. Ramakrishna, Int. J. Hydrogen Energy 37 (2012) 8765–8786.
[35] M. Shen, S. Walter, L. Dovat, M.A.M. Gijs, Microelectron. Eng. 88 (2011) 1884–1886.
[36] P.O. Lopez-Montesinos, N. Yossakda, A. Schmidt, F.R. Brushett, W.E. Pelton, P.J.A. Kenis, J. Power Sources 196 (2011) 4638–4645.
[37] A. Faes, J.M. Fuerbringer, D. Mohamedi, A. Hessler-Wyser, G. Caboche, J. Van herle, J. Power Sources 196 (2011) 7058–7069.
[38] R.H. Myers, A.I. Khuri, W.H. Carter, Technometrics 31 (1989) 137–157.
[39] W. Kleppmann, Taschenbuch Versuchsplanung (2008).
[40] H. Tye, Drug Discov. Today 9 (2004) 485–491.
[41] R.A. Fisher, The Design of Experiments, Oliver & Boyd, Oxford, England, 1951, p. xi, 251.
[42] G.E.P. Box, J.S. Hunter, W.G. Hunter, Statistics for Experimenters: Design, Innovation, and Discovery, Wiley-Interscience, 2005.
[43] JMP® 8 Statistics and Graphics Guide, SAS Institute Inc., Cary, NC, USA, 2009.
[44] E.C. Harrington, Ind. Qual. Control 21 (1965) 494–498.
[45] M. Focke, D. Kosse, D. Al-Bamerni, S. Lutz, C. Müller, H. Reinecke, R. Zengerle, F. von Stetten, J. Micromech. Microeng. 21 (2011) 115002 (11 pp).
[46] C.H. Hamann, A. Hamnett, W. Vielstich, Electrochemistry, Wiley-VCH, Weinheim, 2007. u.a.
[47] H.S. Kim, N.P. Subramanian, B.N. Popov, J. Power Sources 138 (2004) 14–24.
[48] W. Tang, S. Jayaraman, T.F. Jaramillo, G.D. Stucky, E.W. McFarland, J. Phys. Chem. C 113 (2009) 5014–5024.
[49] R.M. Penner, J. Phys. Chem. B 106 (2002) 3339–3353.
[50] S. Kerzenmacher, K. Mutschler, U. Kräling, H. Baumer, J. Ducrée, R. Zengerle, F. von Stetten, J. Appl. Electrochem. 39 (2009) 1477–1485.
[51] S. Trasatti, O.A. Petrii, J. Electroanal. Chem. 327 (1992) 353–376.
[52] J.R.C. Salgado, F. Alcaide, G. Alvarez, L. Calvillo, M.J. Lazaro, E. Pastor, J. Power Sources 195 (2010) 4022–4029.

[53] M.A. Rigsby, W.P. Zhou, A. Lewera, H.T. Duong, P.S. Bagus, W. Jaegermann, R. Hunger, A. Wieckowski, J. Phys. Chem. C 112 (2008) 15595–15601.
[54] S.M. Hwang, J.E. Bonevich, J.J. Kim, T.P. Moffat, J. Electrochem. Soc. 158 (2011) B1019–B1028.
[55] P. Strasser, S. Koha, J. Greeley, Phys. Chem. Chem. Phys. 10 (2008) 3670–3683.
[56] P. Mani, R. Srivastava, P. Strasser, J. Phys. Chem. C 112 (2008) 2770–2778.
[57] J.J. Mallett, U. Bertocci, J.E. Bonevich, T.P. Moffat, J. Electrochem. Soc. 156 (2009) D531–D542.